

Electron Sheaths: The Outsized Influence of Positive Boundaries on Plasmas

B.T. Yee,^{1,*} B. Scheiner,² S.D. Baalrud,² E.V. Barnat,¹ and M.M. Hopkins¹

¹*Sandia National Laboratories, Albuquerque, New Mexico 87185, USA*

²*Department of Physics and Astronomy, University of Iowa, Iowa City, Iowa 52242, USA*

(Dated: July 15, 2019)

Electron sheaths form near the surface of objects biased more positive than the plasma potential, such as in the electron saturation region of a Langmuir probe trace. They are commonly thought to be local phenomena that collect the random thermal electron current, but do not otherwise perturb a plasma. Here, using experiments, particle-in-cell simulations and theory, it is shown that under low temperature plasma conditions ($T_e \gg T_i$) electron sheaths are far from local. Instead, a long presheath region extends into the plasma where electrons are accelerated via a pressure gradient to a flow speed exceeding the electron thermal speed at the sheath edge. This fast flow is found to excite instabilities, causing strong fluctuations near the sheath edge.

A sheath is the space charge region found near the physical boundaries of most plasmas. The vast majority of sheaths are ion rich because this is what naturally forms as highly mobile electrons charge a surface negatively. Comparatively little is known about electrons sheaths, although they are routinely produced when objects are biased positive with respect to the plasma potential [1]. The most common situation is the electron saturation region of a Langmuir probe sweep, but they arise in many other situations including electron sources [2], highly emitting surfaces [3], microdischarges [4], the high potential phase of the rf cycle in processing discharges [5], electron temperature control with wire arrays [6], as well as near probes used for the suppression of turbulence [7], control of the scrape off layer [8], and blob formation [9] in the edge of fusion devices. The conventional understanding from Langmuir probe modeling is that electron sheaths are local phenomena that collect the random electron flux [10–13], but do not otherwise perturb the plasma significantly.

In this Letter, results of experiments, particle-in-cell (PIC) simulations and theory are provided showing that there is in fact a long electron presheath extending into the plasma when the electron temperature significantly exceeds the ion temperature ($T_e \gg T_i$). Furthermore, electrons are accelerated to high velocities in this region, obtaining a distribution that is flow-shifted to a speed exceeding the electron thermal velocity at the sheath edge. This may be considered an electron sheath analog of the Bohm criterion [14]. The fast differential streaming between electrons and ions is found to excite streaming instabilities that give rise to strong fluctuations in the boundary layer region.

Electron presheaths are found to differ in their essential properties from ion presheaths. In particular: (1) the differential potential ($\Delta\phi$) is much smaller, nominally by a factor of T_i/T_e , (2) it is much longer in extent, nominally by a factor of $\sqrt{m_i/m_e}$, but often reaching the discharge dimension, (3) electrons are accelerated by a pressure gradient, in contrast to direct electric field acceleration of ions in an ion presheath, (4) the differential streaming excites instabilities and strong fluctuations, and (5) it has a two-dimensional character that extends into the plasma and causes electrons to funnel into the electron sheath. These results promise new insights into the applications mentioned above. Advances in the fundamental

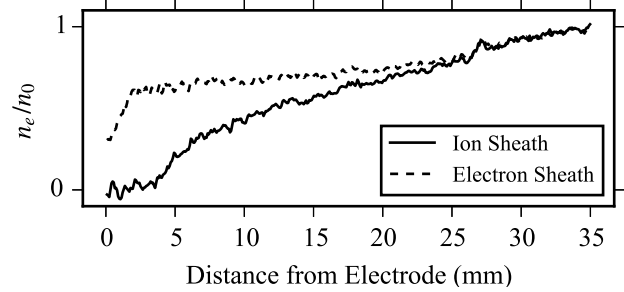


FIG. 1. Measured electron density profiles above the electrode for the ion sheath (solid line) and the electron sheath (dashed line). The bulk density, taken to be at 30 mm, is $3.2 \times 10^9 \text{ cm}^{-3}$ for the ion sheath and $3.3 \times 10^9 \text{ cm}^{-3}$ for the electron sheath.

physics of electron sheaths may also lead to new applications.

Experiments were conducted in a cylindrical vacuum chamber with a setup similar to that in [15]. A 19 mm electrode was used in place of the segmented electrode, and the remainder of the chamber was kept at ground potential. The chamber was filled with 20 mTorr of helium and a plasma was initiated using a barium-impregnated thermionic emitter located 10 cm from the electrode. The electrode was biased to -50 and 15 V, forming an ion sheath and electron sheath respectively. Two-dimensional maps of the electron densities above the electrode were generated using the laser-collisional induced fluorescence (LCIF) diagnostic [16].

Figure 1 shows the axial density profiles from LCIF measurements, normalized by the bulk density, for the ion sheath (solid line) and the electron sheath (dashed line). In both cases, there is a linear density gradient through the bulk plasma. The salient feature is that the presheath can be identified as the region where the electron density profile begins to deviate from the background linear character as the electrode is approached. For the ion sheath case, the sheath is the region from approximately 0–6 mm, and the ion presheath from 6–12 mm. In contrast, the electron sheath is the thin region from 0–2 mm, and the electron presheath from 2–27 mm. This suggests that the electron presheath is much longer in extent than an analogous ion presheath. Furthermore, the electron presheath creates a much larger deviation from the nominal

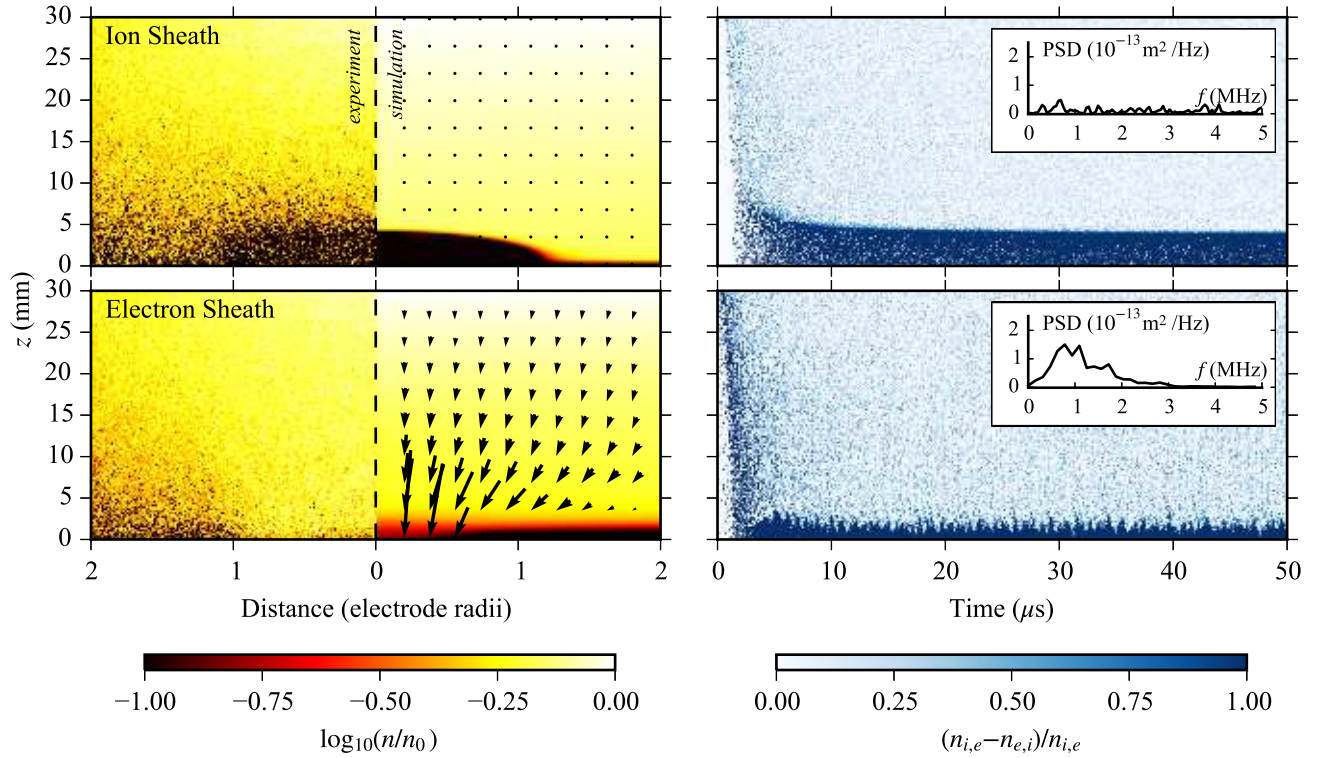


FIG. 2. Experimental and simulated electron density maps (left) and simulated on-axis charge densities over time (right). The ion sheath results comprise the upper plots, and the electron sheath results comprise the lower ones. Overlaid atop the simulated electron densities are the electron current vectors, the magnitudes of which range from $0.1\text{--}1.2 \times 10^{10} \text{ m}^2/\text{s}$ (bulk and sheath edge respectively) for the electron sheath, and below $5 \times 10^8 \text{ m}^2/\text{s}$ for the ion sheath. The power spectral densities of the sheath edge position are inset in the charge density plots.

background density profile than the ion presheath does.

A complementary analysis was carried out using the two-dimensional PIC code, ALEPH [17]. The simulation was conducted in a rectangular Cartesian domain, 75 mm by 50 mm, the same as that used in [18]. However, in this case, the electrode was biased to either -50 V or 15 V to match the experiment. The simulation domain maintains an area ratio of wall to electrode similar to that in the experiment, chosen to assure the formation of an electron sheath [15, 19]. Simulations reached equilibrium after 30 μs while field and particle properties were averaged over an additional 20 μs in order to minimize statistical fluctuation in quantities of interest.

The experimental density measurements are compared to the equivalent simulations in the plots on the left side of Fig. 2. Overlaid on the simulated electron densities are arrows showing the electron current vectors scaled to the same value for both cases. The horizontal axes have been normalized by the electrode radii, in order to provide a more suitable comparison. The right side of Fig. 2 presents maps of the charge density normalized by the density of the collected species. Insets in the charge density maps are power spectra of the sheath position's fluctuations.

In the case of the ion sheath, a large region of electron depletion is visible above the face of the electrode. The size and shape of this region is largely consistent between simulation

and experiment, with the small differences likely ascribable to a discrepancy in the bulk electron densities. An ion sheath is also observed above the grounded wall. Electron current is small throughout the simulated domain and is consistent with the fact that ion sheaths tend to confine electrons. The charge density shows the formation of a stable sheath.

In contrast, the electron sheath simulation in Fig. 2 features a substantial degree of electron current directed toward the electrode from at least as far away as 30 mm. The bulk plasma properties ($n_e = 4.5 \times 10^8 \text{ cm}^{-3}$, $T_e = 2.4 \text{ eV}$) give a Debye length of 0.54 mm, 60 times smaller than the extent of the directed flow. The extent of the flow is consistent with where the density profile from Fig. 1 begins to change slope, indicating the presheath. This consistency suggests that the two-dimensional simulations provide a good foundation upon which to better understand the electron sheath boundary layer. Also notable is the distinctly multi-dimensional nature of the electron presheath. The proximity of the grounded wall to the auxiliary electrode leads to a funnel-like structure in the electron flow with a notable convergence. The electron presheath is clearly a significant perturbation to the plasma. As opposed to the ion sheath, the electron sheath edge exhibits significant fluctuations in its position.

Traditional Langmuir probe analysis assumes that a probe in electron saturation collects the random thermal flux of elec-

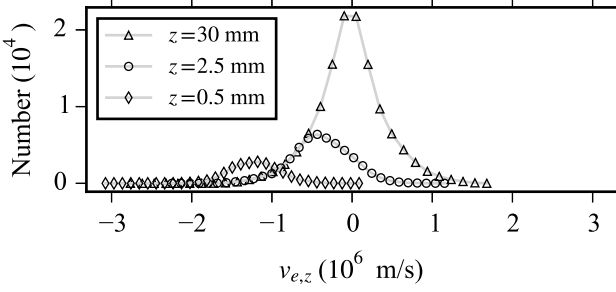


FIG. 3. The electron velocity distribution functions normal to the electrode, along $x = 0$, at several axial locations in the simulations: the injection region (\triangle), the sheath edge (\circ), and inside the sheath (\diamond).

trons incident on the electron sheath. An implication of this local picture is that the electron velocity distribution function (EVDF) at the edge of the electron sheath would be a half-Maxwellian with no flow shift (but with a flow moment) [20]. The random flux of electrons flows into the sheath from the bulk, and all electrons reaching the sheath are lost to the boundary. However, our results show that the presence of an electron presheath leads to a vastly different picture.

In particular, the presheath is found to introduce a substantial flow-shift in the electron distribution, approaching the electron thermal speed by the sheath edge; see Fig. 3. Contrary to the conventional picture of a highly-kinetic truncated distribution function, this figure shows that it is in fact well represented by a flowing Maxwellian. Here, negative velocities indicate electrode-directed electrons. A significant number of electrons flow out of the electron sheath despite the absence of an explicit collision algorithm in the simulations. The sheath is defined as where quasineutrality is sufficiently violated, or $(n_e - n_i)/n_e = \epsilon$ where we have chose $\epsilon = 0.3$ in order to avoid stochastic density variations in the bulk plasma. This approach places the sheath edge at $z = 2.0$ mm. More is said of this choice for ϵ below, in view of the strong density fluctuations in this region.

Motivated by the Maxwellian EVDFs, a fluid analysis is used to interpret aspects of the experiments and simulations. One interesting feature is the acceleration mechanism of electrons. Consider the fluid momentum balance

$$u_e \frac{du_e}{dz} = -\frac{eE}{m_e} - \frac{k_B T_e}{m_e n_e} \frac{dn_e}{dz} - u_e(\nu_c + \nu_s) \quad (1)$$

where e is the elementary charge, E is the electric field, ν_c is the collision frequency, and ν_s represents the source (ionization) frequency. The terms on the right-hand side represent the forces due to the electric field, pressure gradient, and collisions respectively. The largest of these terms is the pressure gradient term. Taking the ion density to vary according to the Boltzmann density relation,

$$\frac{eE}{k_B T_i} = \frac{1}{n} \frac{dn}{dz}. \quad (2)$$

Substituting this into Eq. (1) shows that the pressure gradient

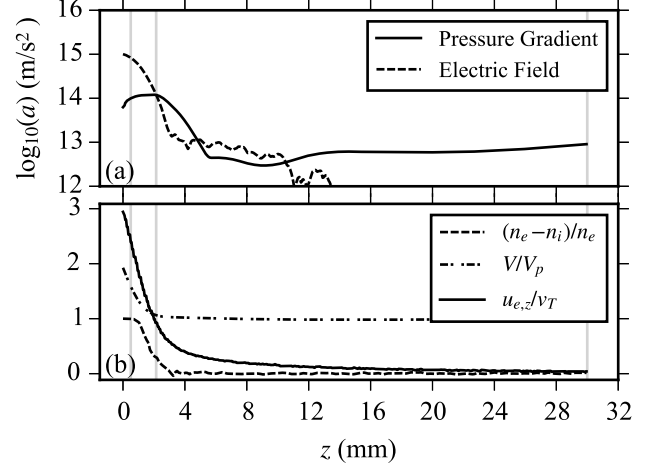


FIG. 4. (a) Pressure gradient (solid line) and the electric field (dotted line) accelerations obtained from simulations. The solid gray lines indicate the locations where the EVDFs in Fig. 3 were obtained, with the middle line indicating the location of the sheath edge. (b) Normalized charge density (dashed line), the electron fluid velocity (solid line), and potential (dash-dotted line) in the direction normal to the electrode surface, with respect to the distance from the electrode along $x = 0.0$.

term is T_e/T_i larger than the electric field. Although the potential gradient in the presheath is small (characterized by T_i), the resulting pressure gradient drives a strong electron flow due to the steep density gradient that results. This contrasts with the situation found in ion presheaths, where the electric field term exceeds the pressure gradient term by T_e/T_i , and the presheath potential drop is of the order of T_e (rather than T_i). In this case, ions are accelerated ballistically by the electric field to a speed exceeding the sound speed at the sheath edge. The importance of the pressure gradient term with respect to the electric field is confirmed in the simulations. Figure 4(a) plots the pressure gradient (solid line) and electric field (dashed line) acceleration terms from Eq. (1) on a logarithmic scale, as a function of distance from the electrode.

The simulations indicate that the pressure gradient is the dominant acceleration mechanism from 2–5 mm and $z > 11$ mm. The drop in pressure gradient between 5 mm and 11 mm coincides with a plateau in the simulated electron density near the sheath edge (similar to that seen in Fig. 1) and a plateau in electron temperature (not shown). Several factors may contribute to this plateau including a stagnation of ions as they approach the sheath potential barrier and a change in the convergence of the electron fluid. Past 11 mm, the pressure gradient continues to dominate the acceleration of the electron fluid up to the sheath edge.

The degree to which the electron fluid is accelerated can be calculated via the electron continuity equation

$$\frac{d}{dz}(n_e u_e) = \nu_s n_e, \quad (3)$$

and a common sheath criterion, which identifies the sheath

edge as the location where $\sum q dn/dz \leq 0$ [21], where q is the charge of the species. Dropping the collision terms, Eqs. (1) and (3) yield $dn_e/dz = en_eE/(m_eu_e^2 - k_B T_e)$. From Eq. (2), and assuming quasineutrality, the sheath criterion provides an electron-sheath analog of the Bohm criterion,

$$u_e \geq \sqrt{\frac{k_B(T_e + T_i)}{m_e}} \equiv v_T. \quad (4)$$

A similar derivation of the electron fluid speed at the sheath edge was previously obtained by Loizu, Dominski, Ricci, and Theiler [22]. This criterion demands a region of electron acceleration outside of the sheath region.

Figure 4(b), shows the charge density (dashed line), the electron fluid velocity (solid line), and the local potential (dash-dotted line). The electron fluid is found to reach a velocity of $0.92v_T$ by the sheath edge (as previously defined), in fair agreement with Eq. (4). A number of factors may contribute to the remaining discrepancy including the ambiguity in the definition of a precise sheath edge location [18], the use of a planar one-dimensional theory in describing a converging flow, and the substantial fluctuations observed in the simulations near the sheath edge.

The fast electron flow creates a large differential streaming between electrons and ions that is expected to lead to ion-acoustic instabilities [23] in the electron presheath. Indeed, Fig. 2 shows substantial density fluctuations are observed near the electron sheath edge, but not in the case of the ion sheath simulation. The frequency of these fluctuations is observed to peak around 0.8 MHz comparable to the most unstable mode of ion-acoustic instability (ion plasma frequency) which is 1.4 MHz (using the ion density at $z = 2.0$ mm, $1.7 \times 10^8 \text{ cm}^{-3}$). In addition, it is observed that the ion flow obtains a radial component near the sheath edge, which may contribute to ion-ion two-stream instabilities [24]. The presence of these strong fluctuations blurs the sheath edge location, as shown in Fig. 2. In a steady-state sense, a transition region is formed between presheath and sheath as a result of the fluctuations. The previous estimate of the sheath edge (at $z = 2.0$ mm) was based on where the time-average charge density is reduced by 30% (if instead an estimate based on the Child-Langmuir sheath thickness is used, Eq. (13) of [13], an estimate of $z = 1.5$ mm is obtained [25]).

The length scale of an ion presheath is typically determined by collisional processes, and is estimated as the ratio of the ion flow speed to the collision frequency $l_i \simeq c_s/\nu$ for a specific process such as ionization. The electron presheath length would be estimated to be $l_e \simeq v_T/\nu$. This implies that, for the same collision process, the electron presheath is much longer than the ion presheath, by a factor of

$$\frac{l_e}{l_i} = \frac{v_T}{c_s} = \sqrt{\frac{T_e + T_i}{m_e}} \frac{m_i}{T_e} \approx \sqrt{\frac{m_i}{m_e}}. \quad (5)$$

As an example, $l_e/l_i \approx 270$ in argon or $l_e/l_i \approx 85$ in helium. For a typical low temperature plasma experiment, the

presheath length may be constrained by the dimensions of the plasma rather than the collision mean free path. Figures 1 and 2 support the suggestion that electron presheaths are much longer than ion presheaths. This is a very different picture than the assumption of a local phenomenon that is found in Langmuir probe theory.

These novel properties of the electron sheath are surprising both because of how they differ from ion sheaths and because of their influence on the bulk plasma. The perturbations in electron density and flow caused by what would otherwise be considered a small electrode suggests that conventional models of electron sheaths need to be revisited. These fundamental physics results may also lead to useful new applications.

This work was supported by the Office of Fusion Energy Science at the U.S. Department of Energy under contracts DE-AC04-94SL85000 and de-sc0001939.

* btyee@sandia.gov

- [1] I. Langmuir, Phys. Rev. **33**, 954 (1929).
- [2] B. Longmier, S. D. Baalrud, and N. Hershkowitz, Rev Sci. Instrum. **77** (2006), 10.1063/1.2393164.
- [3] M. D. Campanell, Phys. Rev. E **88**, 033103 (2013).
- [4] Q. Wang, D. J. Economou, and V. M. Donnelly, J. Appl. Phys. **100** (2006), 10.1063/1.2214591.
- [5] C. M. O. Mahony, R. Al Wazzan, and W. G. Graham, Appl. Phys. Lett. **71**, 608 (1997).
- [6] C.-S. Yip and N. Hershkowitz, Plasma Sources Sci. Technol. **24**, 034004 (2015).
- [7] B. Richards, T. Uckan, A. J. Wootton, B. A. Carreras, R. D. Bengtson, P. Hurwitz, G. X. Li, H. Lin, W. L. Rowan, H. Y. W. Tsui, A. K. Sen, and J. Uglum, Phys. Plasmas **1**, 1606 (1994).
- [8] S. J. Zweben, R. J. Maqueda, A. L. Roquemore, C. E. Bush, R. Kaita, R. J. Marsala, Y. Raitses, R. H. Cohen, and D. D. Ryutov, Plasma Phys. Control. Fusion **51**, 105012 (2009).
- [9] C. Theiler, I. Furno, J. Loizu, and A. Fasoli, Phys. Rev. Lett. **108**, 065005 (2012).
- [10] H. Mott-Smith and I. Langmuir, Phys. Rev. **28**, 727 (1926).
- [11] G. Medicus, J. Appl. Phys. **32**, 2512 (1961).
- [12] B. E. Cherrington, Plasma Chem. Plasma P. **2**, 113 (1982).
- [13] N. Hershkowitz, Phys. Plasmas **12**, 055502 (2005).
- [14] D. Bohm, in *The Characteristics of Electrical Discharges in Magnetic Fields*, edited by A. Guthrie and R. K. Wakerling (McGraw-Hill, New York, NY, 1949) Chap. 3, p. 77.
- [15] E. V. Barnat, G. R. Laity, and S. D. Baalrud, Phys. Plasmas **21**, 103512 (2014).
- [16] E. V. Barnat and K. Frederickson, Plasma Sources Sci. T. **19**, 055015 (2010).
- [17] H. Timko, P. S. Crozier, M. M. Hopkins, K. Matyash, and R. Schneider, Rev. Sci. Instrum. **65**, 140 (2012).
- [18] S. D. Baalrud, B. Scheiner, B. T. Yee, M. M. Hopkins, and E. V. Barnat, Plasma Phys. Contr. F. **57**, 044003 (2015).
- [19] S. D. Baalrud, N. Hershkowitz, and B. Longmier, Phys. Plasmas **14**, 042109 (2007).
- [20] K.-U. Riemann, Phys. Fluids **24**, 2163 (1981).
- [21] K.-U. Riemann, J. Phys. D **24**, 493 (1991).
- [22] J. Loizu, J. Dominski, P. Ricci, and C. Theiler, Phys. Plasmas **19**, 083507 (2012).
- [23] P. Bellan, in *Fundamentals of Plasma Physics* (Cambridge Uni-

versity Press, Cambridge, UK, 2006) p. 177.

[24] A detailed analysis of the fluctuation spectrum will be provided in a later publication.

[25] In his paper, Hershkowitz identifies Eq. (17) as the one to be

used for electron sheaths, however this expression assumes only random thermal electron flux enters the sheath. Given the observed flow shift, Eq. (13) is considered the more appropriate choice.